Journal of
Micro/Nanolithography, MEMS, and MOEMS

SPIEDigitalLibrary.org/jm3

# Mask replication using jet and flash imprint lithography

Kosta S. Selinidis
Cynthia B. Brooks
Gary F. Doyle
Laura Brown
Chris Jones
Joseph Imhof
Dwayne L. LaBrake
Douglas J. Resnick
S. V. Sreenivasan

SPIE

# Mask replication using jet and flash imprint lithography

**Kosta S. Selinidis**
**Cynthia B. Brooks**
**Gary F. Doyle**
**Laura Brown**
**Chris Jones**
**Joseph Imhof**
**Dwayne L. LaBrake**
**Douglas J. Resnick**
**S. V. Sreenivasan**
Molecular Imprints, Inc.
1807-C West Braker Lane
Austin, Texas 78758
E-mail: dresnick@militho.com

**Abstract.** The jet and flash imprint lithography (J-FIL™) process uses drop dispensing of UV curable resists to assist high resolution patterning for subsequent dry etch pattern transfer. The technology is actively being used to develop solutions for memory markets including flash memory and patterned media for hard disk drives. It is anticipated that the lifetime of a single template (for patterned media) or mask (for semiconductors) will be on the order of $10^4$ to $10^5$ imprints. This suggests that tens of thousands of templates/masks will be required to satisfy the needs of a manufacturing environment. Electron-beam patterning is too slow to feasibly deliver these volumes, but instead can provide a high quality master mask which can be replicated many times with an imprint lithography tool. This strategy has the capability to produce the required supply of "working" templates/masks. In this paper, we review the development of the mask form factor, imprint replication tools, and the semiconductor mask replication process. A Perfecta™ MR5000 mask replication tool has been developed specifically to pattern replica masks from an e-beam written master. Performance results, including image placement, critical dimension uniformity, and pattern transfer, are covered in detail.  [DOI: 10.1117/1.3646523]

Subject terms: jet and flash imprint lithography; mask; replication; high contrast mark.

Paper 11079PR received Jun. 16, 2011; revised manuscript received Aug. 30, 2011; accepted for publication Sep. 15, 2011; published online Oct. 21, 2011.

## 1 Introduction

The jet and flash imprint lithography (J-FIL™) process uses drop dispensing of UV curable resists to assist high resolution patterning for subsequent dry etch pattern transfer.[1–7] The technology is actively being used to develop solutions for memory markets including flash memory and patterned media for hard disk drives. It is anticipated that the lifetime of a single template (for patterned media) or mask (for semiconductors) will be on the order of $10^4$ to $10^5$ imprints. This suggests that tens of thousands of templates/masks will be required to satisfy the needs of a manufacturing environment. Electron-beam patterning is too slow to feasibly deliver these volumes, but instead can provide a high quality master mask which can be replicated many times with an imprint lithography tool.

Previous work on patterned media for hard drives has demonstrated the feasibility of replicating templates for both discrete track recording and bit patterned media. A typical process flow is shown in Fig. 1. Replication of the master was conducted using a Perfecta 1100TR system. The TR1100 uses Molecular Imprint's J-FIL™ technology and was specifically designed to produce templates meeting the requirements for patterned media disk imprinting systems. The TR1100 system capabilities include micrometer level alignment, template automation, and the ability to handle 150 mm fused silica substrates. The system can produce approximately 10 replica (or working) templates per hour, more than 2 orders of magnitude more productive than today's leading edge e-beam template writers.

For the case of the semiconductor market, a variety of feature types must be resolved, although for most memory applications, the dominant feature set consists of 1:1 line/space patterns for critical front-end layers, particularly Flash. In the case of Flash memory, the most aggressive production designs are now pushing to half pitches of 25 nm and below. For such designs, mask critical dimension uniformity (CDU) must be less than 10% of the minimum device half pitch, mask image placement must be below 5 nm, and defectivity of the mask is required to be less than 1 defect/cm$^2$. In this paper, we review the development of the mask form factor, the semiconductor mask imprint tool, and imprint process. Details on CDU, image placement, and pattern transfer specifically for semiconductor replica masks are also discussed.

The requirements needed for semiconductors dictate the need for a well-defined form factor for both master and replica masks which is also compatible with the existing mask infrastructure established for the 6025 semistandard, $6'' \times 6'' \times 0.25''$ photomasks. Complying with this standard provides the necessary tooling needed for mask fabrication processes, cleaning, metrology, and inspection. The replica form factor has additional features specific to imprinting such as a prepatterned mesa. A Perfecta™ MR5000 mask replication tool has been developed specifically to pattern replica masks from an e-beam written master. Along with the tool, a new process has been developed to fabricate replicas with high contrast alignment marks so that designs for imprint can fit within current device layouts and maximize the usable printed area on the wafer. Initial performance results

1932-5150/2011/$25.00 © 2011 SPIE

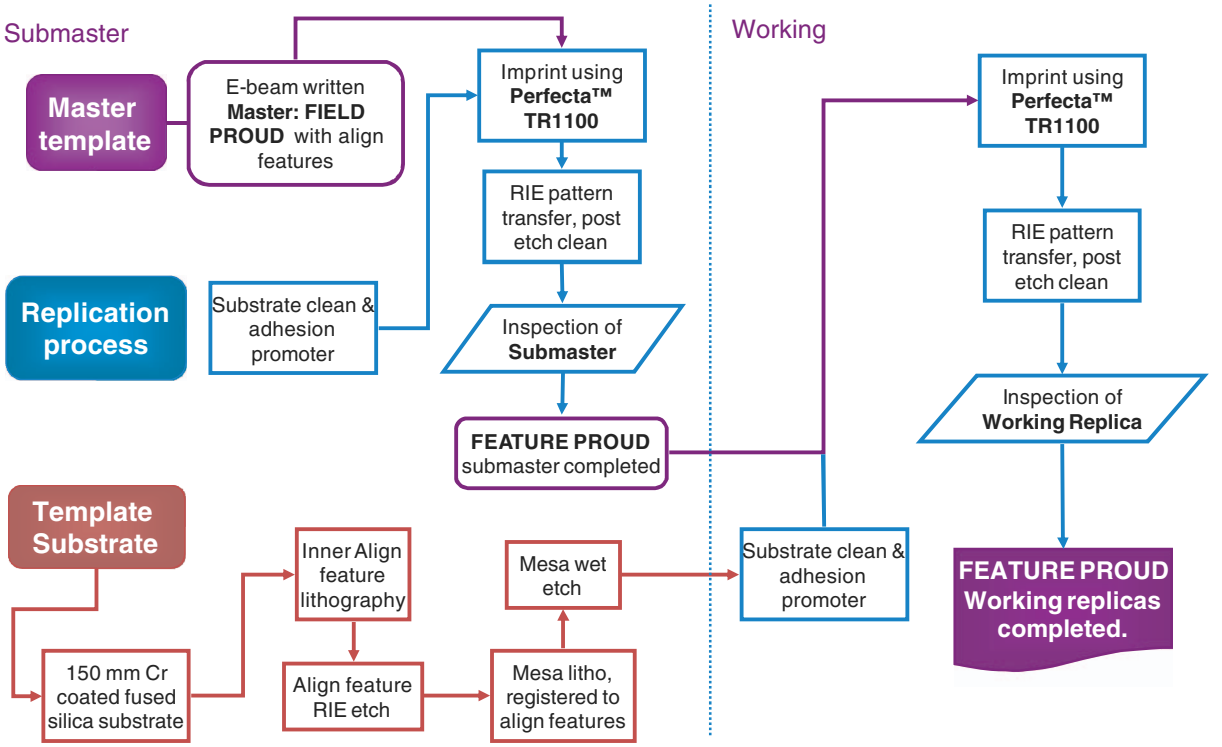


**Fig. 1** Process flow for creating both submaster and working replica templates for patterned media.

with this mark are comparable to the baseline fused silica align marks.

## 2 Mask Details

### 2.1 *Mask Form Factor*

The 6025 master mask form factor allows mask shops to use the identical tooling currently used for resist coating, writing, patterning pattern transfer, metrology, inspection, and repair. Unlike standard photomasks which required the majority of the mask surface to achieve a 4× reduction, imprint replication is a 1:1 patterning process and only requires the very middle of the mask for patterning the features within a field. The additional space around the periphery of the device patterns is used for registration marks in order to align the pattern to the mesa on the replica mask blank.

The replica mask also has a 6025 form factor, but additionally includes a raised pedestal or mesa (see Fig. 2.). This mesa later becomes the patterned area of the replica mask. This design was chosen specifically to eliminate the defects added to the mask by forming the mesa after the pattern transfer of the fine features on the mesa. As a result, we can take advantage of the imprint blank infrastructure that has already demonstrated an imprint mask blank defectivity of only 0.04/cm$^2$.[8]

### 2.2 *Mask Replication Tooling and Processing*

The MR5000 is an imprint tool designed specifically for semiconductor mask replication. The tool accepts a standard 6025 mask form factor and prints field sizes ranging from a minimum of 13 mm × 13 mm to a maximum of 26 mm × 33 mm. Throughput is 4 masks/h, and residual layer thickness uniformity (RLTU) and the added critical dimension uniformity error are specified as 5 nm and 0.3 nm, 3$\sigma$, respectively. The added image placement error is specified at 5 nm, 3$\sigma$, and the tool operates within an ISO Class 2 environment.

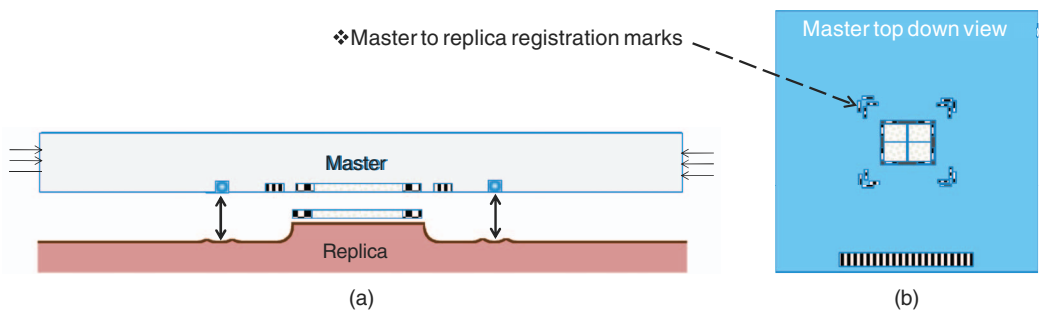


**Fig. 2** (a) A schematic of the process used to align the master mask to the replica mask blank. Registration marks outside of the active field aid in the alignment of the field to the mesa on the replica. (b) Schematic illustration of the patterned master mask.

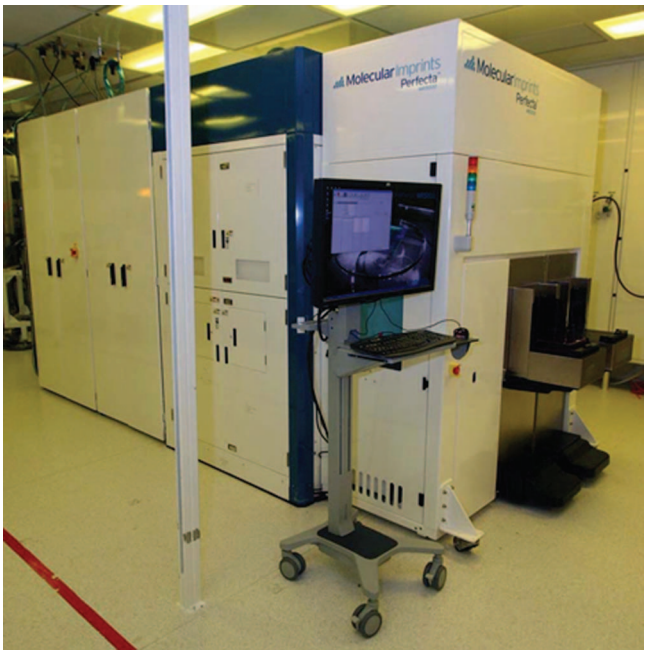

**Fig. 3** Photograph of the MR5000 mask replication tool.

A photograph of the MR5000 is shown in Fig. 3. The tool is modular in design and consists of four major subsections. Moving from right to left in Fig. 3 are the equipment front end module (EFEM), the imprint chamber, the service corridor, and the environmental control unit. The EFEM contains two load ports configured to handle standard 6025 reticle SMIF pods. Within the EFEM are 20 shelves designed for acclimating both the loaded master and replica blanks. The master mask chuck is surrounded by a force feedback magnification actuator system which is designed to correct both magnification and systematic distortion errors.[9] Resist is dispensed using ink jet heads at volumes of less than 6 pl/nozzle. Ink jet drop patterns are defined by an IntelliJet$^{TM}$ software system designed to match the volume of resist to the GDS pattern layout of the master mask.[9]

The replication process flow is shown in Fig. 4.[10,11] Prior to imprinting the replica blank, an adhesion layer is applied. The adhesion layer provides preferential bonding between the replica blank and the imprint resist which is critical for maintaining low defectivity during the imprint process. Properties of this vapor adhesion layer (VALMat) layer have been discussed in detail in previous publications.[12,13] Briefly, VALMat was specifically designed to have low molecular weight and high vapor pressure at room temperature. This is a preferred method for coating, since vapor deposition processes can achieve excellent uniformity and low defectivity across the mesa of the replica blank.

Adjustment of magnification is done within the imprint tool by registering the master to a reference. This extra step provides additional flexibility to better meet customer overlay requirements. After the resist image is imprinted onto the replica blank, pattern transfer is accomplished by plasma etching in series the remaining resist residual layer (<15 nm), the chromium hard mask, and underlying fused silica. A schematic of the pattern transfer process along with representative SEM images are shown in Fig. 5.

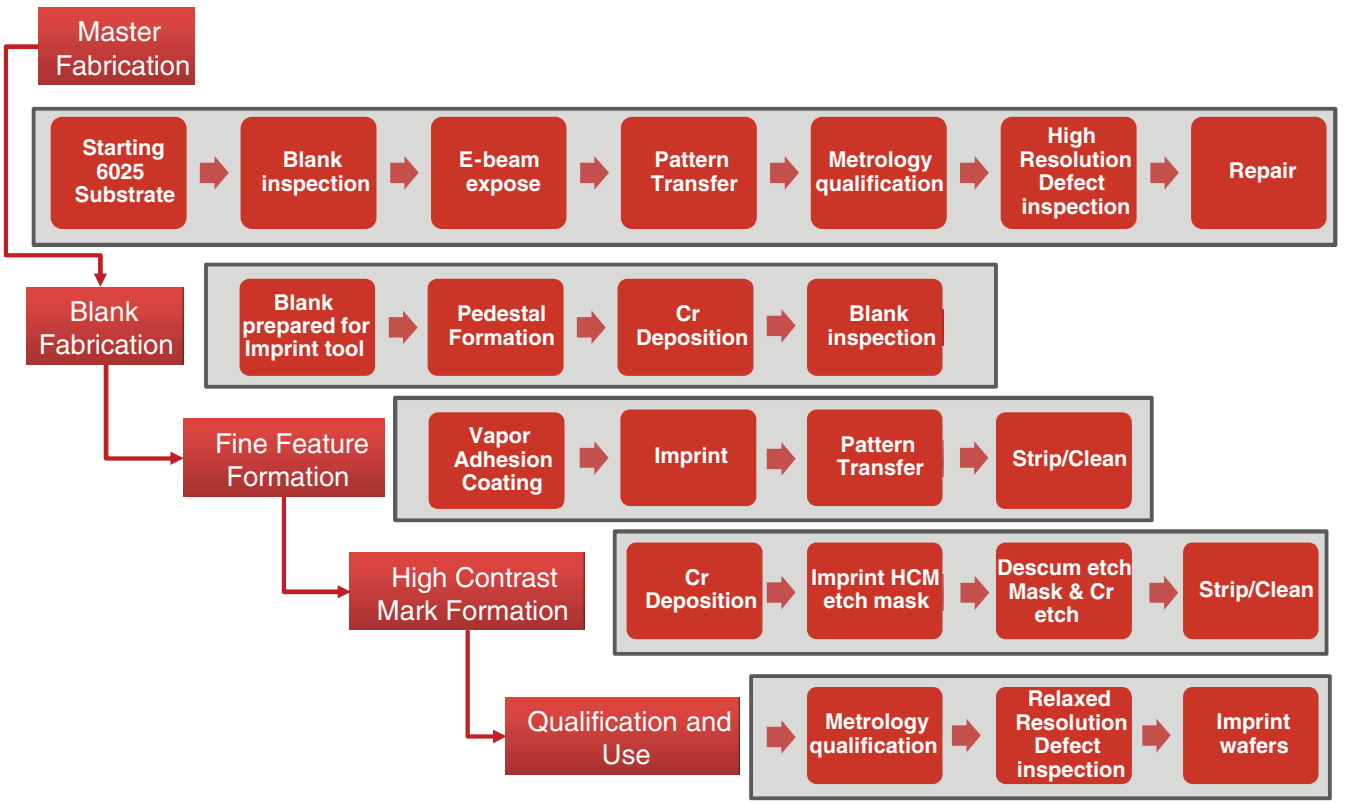


**Fig. 4** Replica process flow, including steps for master fabrication, replica blank formation, fine feature patterning, high contrast mark definition, and replica mask qualification and use.

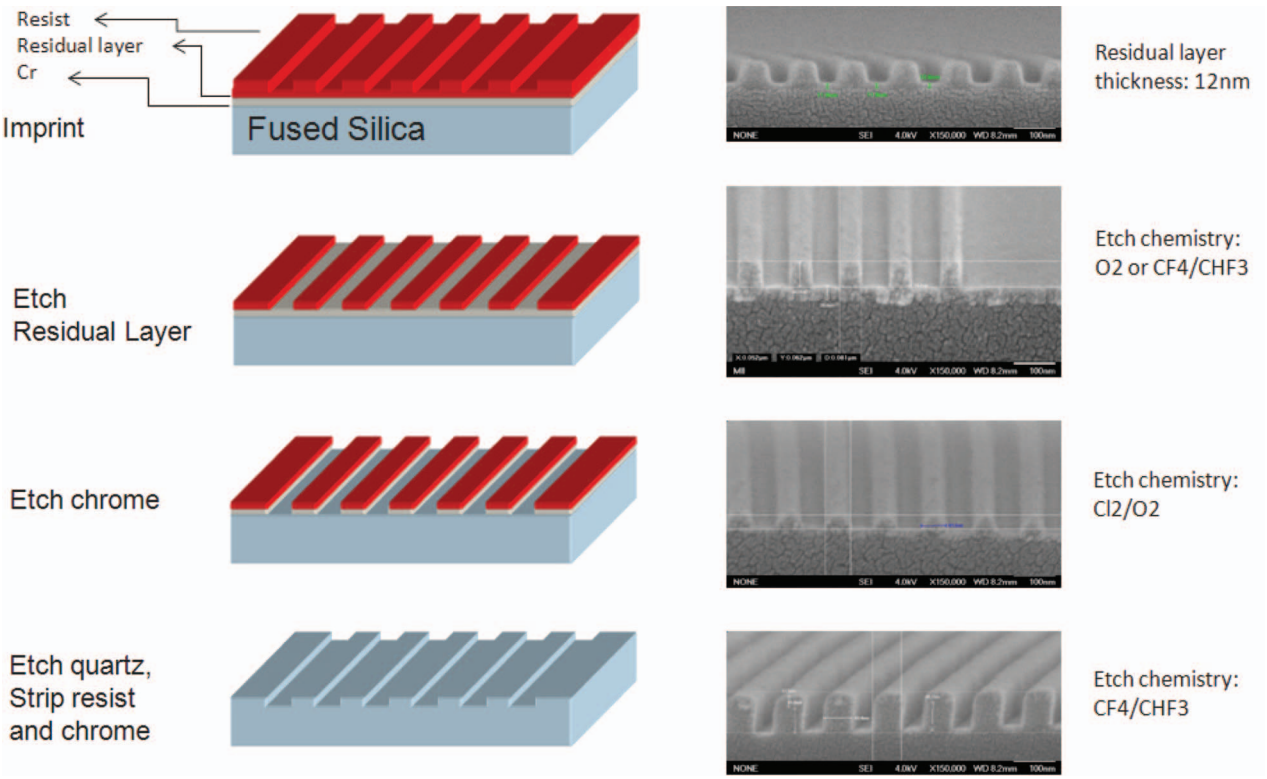


**Fig. 5** Key processing steps necessary for replica pattern transfer.

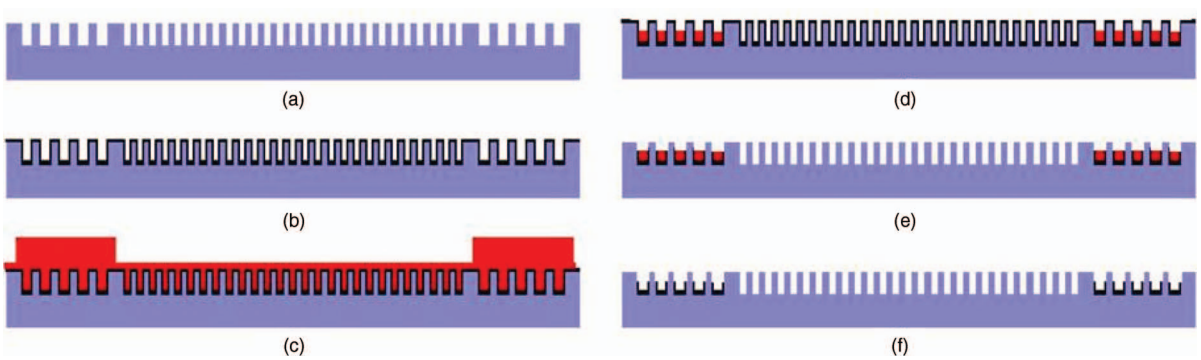


**Fig. 6** High contrast mark process flow: (a) patterned replica mask; (b) thin chromium deposition; (c) imprint step to isolate the alignment features; (d) resist etchback; (e) chromium wet etch; (f) resist strip.

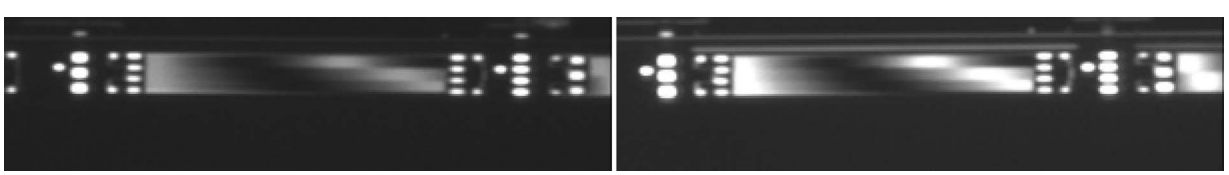

**Fig. 7** Moiré signal intensity using a thin (10 nm) and thick (30 nm) chromium layer.

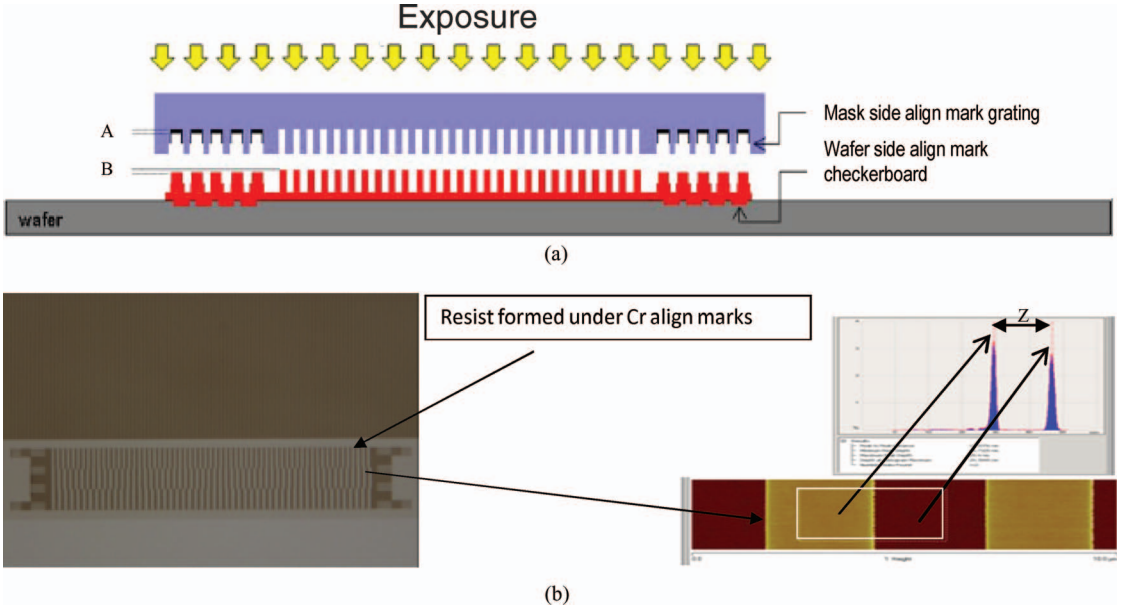


**Fig. 8** (a) Cross-sectional view of a recessed chromium mask during wafer imprinting. (b) Resist pattern on a silicon wafer demonstrating patterning under the chromium material, along with an AFM histogram of the resist height.

The final steps in the process include a high contrast mark (HCM) fabrication sequence and metrology and inspection. Inspection has been discussed in previous publications.[14,15] Details of the HCM steps are reviewed in Sec. 3.

## 3 Replication Results

### 3.1 *High Contrast Align Mark Formation*

MII CMOS wafer imprint tools use a Moiré alignment scheme to align the mask to patterns on the wafer.[16] Typically the mask pattern contains a periodic line/space structure and the wafer substrate has a corresponding checkerboard pattern. The interaction between these mask and wafer features scatter light in such a way that results in an optical image providing subnanometer resolution alignment information. The original Moiré align mark design included a moated area to separate the imprint resist in the patterned area from the align mark.[17] This was necessary because the imprint fluid has a very similar index of refraction to the fused silica. As a result, features in the mask would become invisible when in contact with the resist fluid and thus the Moiré align technique would not function properly. By creating an air gap (with an index of refraction of 1.00), the mark was easily viewed. While acceptable for research and development, the approach has two drawbacks: 1. the moated area takes up valuable real estate on the field which can no longer be patterned, and 2. the moated area is subject to contamination from the nearby deposited resist drops, which may affect alignment signal strength after printing several wafers.[18]

The moat has been eliminated by depositing a thin (~15 nm) layer of chromium in the base of the trenches of the Moiré mark on the replica mask. The chromium film provides contrast when the liquid resist fills the Moiré relief images, thereby enabling a high intensity interferometric signal. While many different materials are possible for use with an HCM scheme, chromium has been selected for its compatibility with both standard photomask processing and imprint processing. The method for fabricating the HCM is shown in Fig. 6. After patterning of the fine features, chromium is deposited across the field [Fig. 6(b)]. An imprint step is then used to apply a uniform layer of resist across the field while preferentially protecting the alignment mark locations [Fig. 6(c)]. This step is important because typical resist planarization methods such as spin-on techniques do not work uniformly over large mesa edges. A resist etch-back step exposes the chromium in all areas except the align marks [Fig. 6(d)], then chromium is selectively removed [Fig. 6(e)] and the remaining resist is stripped away [Fig. 6(f)]. Two examples of Moiré signals are shown in Fig. 7. Both thin (10 nm) and thick (30 nm) chromium layers were tested, and both signal intensities were found to be greater than the baseline Moiré signal observed in air.

Although chromium is a good material for producing a Moiré signal with high contrast, there was an initial concern that this material might interfere with resist curing. As shown

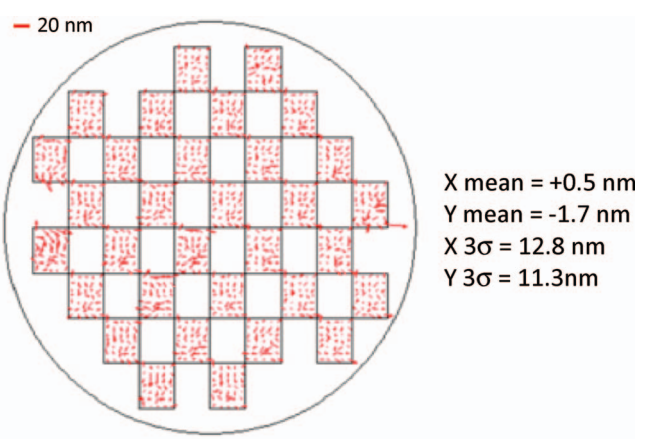


**Fig. 9** Mix and match overlay achieved using an HCM imprint mask.

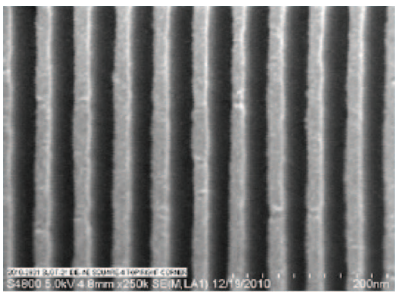

(a)

| CDU 3σ | Imprint 1 (nm) | Imprint 2 (nm) | Master (nm) |
|---|---|---|---|
| 28nm | 1.9 | 1.9 | 1.9 |
| 24nm | 1.8 | 1.8 | 1.3 |

(b)

**Fig. 10** (a) Example of imprinted 24 nm half pitch lines using the MR5000 tool. (b) 3$\sigma$ error comparison between the master mask and two replica masks.

in Fig. 8(a), UV light passes through the glass to expose the resist. If the chromium in the align mark absorbs or reflects too much light, then the resist under the align mark may not cure properly. In this condition, the resist will be more prone to evaporation and shrinkage, and may act as a potential contamination source.

To evaluate the resist exposure beneath the high contrast marks, an experiment was run with four different Moiré mark conditions: No chromium, 10 nm, 15 nm, and 30 nm chromium thicknesses. An AFM was used to scan across the imprinted feature of resist which directly corresponds to the align mark areas with chromium. Figure 8(b) shows the imprinted resist pattern and an example of an AFM scan. The two-dimensional image of the AFM scan depicts the height of resist as a brightness change. The feature height is measured by creating a histogram of the image brightness inside the white box as shown. The distance between the two dominant peaks indicates the step height, $z$, of the resist. The resist patterned under the align mark is then compared to the resist outside of the align mark. After accounting for the thickness of the chromium [shown as A and B in Fig. 8(a)], we can make an assessment of the impact of chromium within the align marks.

In all cases, resist under the align marks was properly cured with the target exposure dose of 100 mJ/cm$^2$. Some resist thickness loss was observed for the 30 nm Cr thickness at exposure doses below 80 mJ/cm$^2$. This is an extreme case, however, and only serves to define the limits of the process. Thicknesses around 15 nm showed optimal contrast with no adverse effects from chromium shadowing as compared to the no chromium condition.

Alignment and overlay were tested by placing a mask with high contrast marks on an Imprio 500 and aligning to a silicon wafer patterned with a 193 nm scanner. The results are shown below. Three $\sigma$ mix-and-match errors were 12.8 nm in $x$ and 11.3 nm in $y$, less than the 15 nm overlay specification on the tool (see Fig. 9). It should be noted that the imprint mask used for this test had image placement errors of approximately 10 nm, indicating that better mix and match results should be obtained by using an imprint mask with smaller image placement errors.

### 3.2 *Imprint Characterization*

Initial data has been collected to evaluate the performance of the MR5000. First tests include CDU, residual layer thickness uniformity, and image placement error contributions.

CDU was tested by measuring 24 and 28 nm dense lines at 30 different locations on both the master and replica mask and comparing the 3$\sigma$ variations for each data set. The results are shown in Fig. 10. The 28 nm features for both the master and

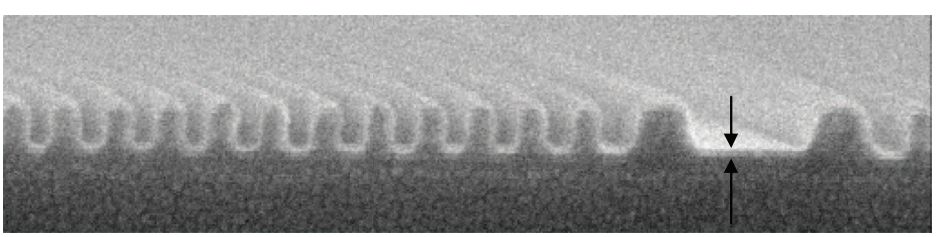

(a)

| | RLT Mean | RLT 3σ |
|---|---|---|
| Field to Field | 10.6nm | 1.6nm |
| With-in Field | 10.3nm | 1.5nm |

(b)

**Fig. 11** (a) Imprint cross section showing both the feature cross section and the residual resist layer. (b) Within-field and field to field RLT and RLTU.

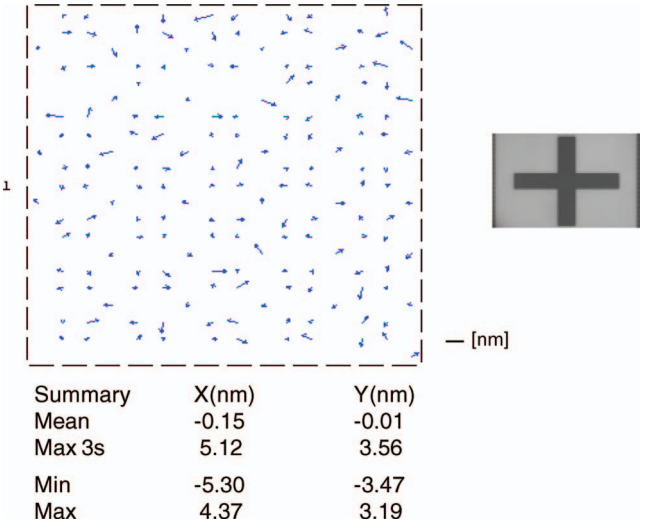


**Fig. 12** Image placement vector plot showing the added image placement error contribution resulting from the mask replica process after imprinting. The mark used to measure the displacement vectors with an IPRO1 is shown to the right of the vector plot. Dimensions of the mark are 5 $\mu$m in width and 30 $\mu$m in height.

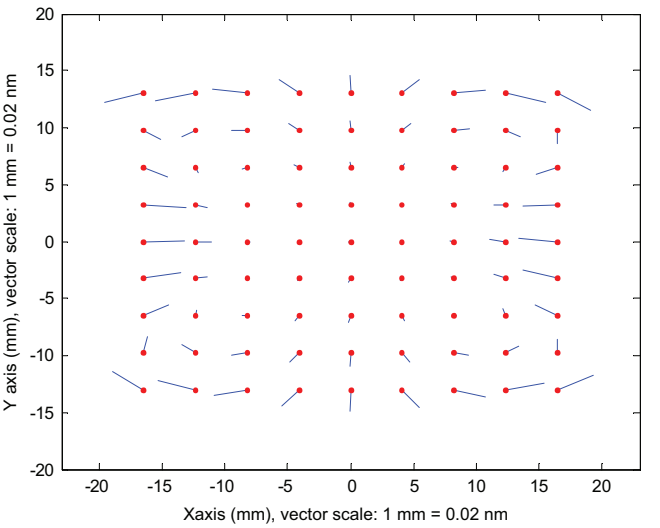


**Fig. 13** Induced distortion per ppm applied magnification correction. Maximum error vectors in *x* and *y* are 0.07 and 0.04 nm, respectively.

replica show no difference in the $3\sigma$ variation. The master and replica differ by 0.5 nm for the 24 nm lines. The error differences are within the gauge capability of the SEM, and consistent with previous work that documents that little or no additional variation occurs as a result of imprinting.[19]

Residual layer thickness (RLT) and RLTU tool specifications are $<$15 nm and $<$5 nm, $3\sigma$, respectively. To test the MR5000 RLT performance, three mask fields were imprinted. Data from each field were collected by cleaving each field in 3 locations, and measuring the RLT with an SEM in 15 locations across the width of each field. This resulted in a data set consisting of 45 SEM RLT measurements for each field. The measured average RLT within-field for one of the fields was 10.3 nm. To calculate the field to field variation, the RLT data for all three imprinted samples was combined and analyzed, resulting in an average RLT of 10.6 nm. The RLTU for a single field and all three fields was 1.5 and 1.6 nm, respectively. An example of a resist cross section and a summary chart of the RLT data are shown in Fig. 11.

Image placement errors were evaluated by measuring both a master mask and an imprinted mask and comparing the

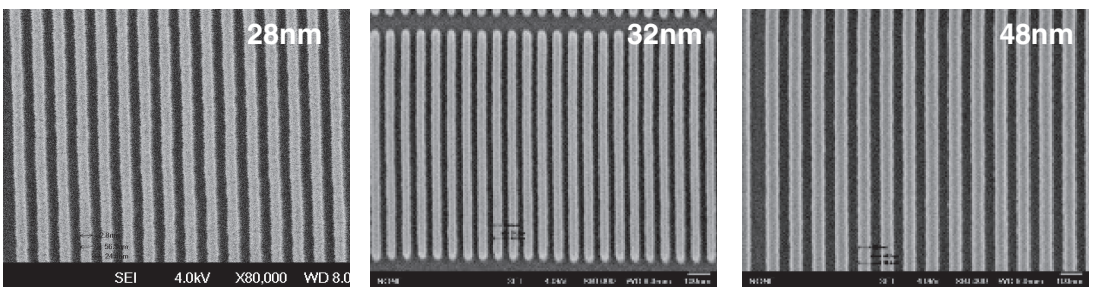


(a) Master Imprint

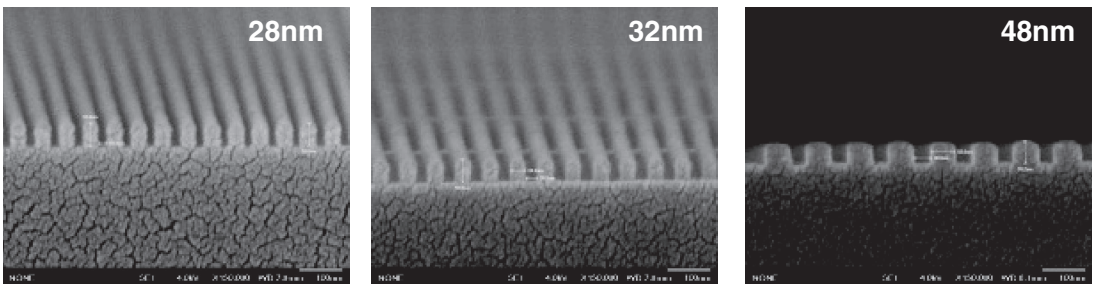


(b) Replica Mask

**Fig. 14** Pattern transfer of a semiconductor replica mask. (a) Imprints of the master onto the mesa of the replica substrate. (b) The same features etched into the replica mask.

image placement vectors. Measurements were made on a Leica IPRO1. The gauge error on this tool is estimated at 3 to 4 nm. The added image placement error vector plot is shown in Fig. 12. The added contributions to image placement are 5.12 nm in $x$ and 3.56 nm in $y$. The added error contributions will need to eventually be reduced to approximately 2 nm in order to meet the requirements of the ITRS roadmap. It should be noted that modeling indicates that the error contribution from compressing the mask is not more than 0.07 nm per ppm of applied magnification correction (see Fig. 13). Additional experiments and modeling will be required to identify the key contributors and drive image placement down to acceptable levels.

### 3.3 *Replica Mask Pattern Transfer*

In order to study pattern transfer, a master mask was fabricated by DNP. The field size was 26 ×32 mm, and contained critical dimensions of 28, 32, and 48 nm. For this work, fluorine-based chemistry was used to etch the residual layer in order to minimize CD loss during pattern transfer. Pattern transfer examples of all three feature sizes are shown in Fig. 14. Figure 14(a) shows the imprints from the master. Figure 14(b) shows cross-sections of the same features on the replica mask. Note the near vertical profile obtained for all three line sizes. A cursory study of etch depth uniformity looks promising. A targeted 60 nm fused silica etch resulted in an etch depth of 60.5 nm, with a $3\sigma$ variation of only 2.5 nm.[20] A more detailed study of both etch depth uniformity and CDU after etch will be the subject of future studies.

## 4 Conclusions

A first look has been taken at the replication of semiconductor masks. A semiconductor mask specific replication tool, the MR5000, has been fabricated, shipped to DNP, and the initial data is promising. A high contrast mark process has been developed in order to maximize wafer pattern area and insure longevity during field to field alignment. Critical dimension uniformity and residual layer thickness uniformity are performing well within tool specifications. An initial study of image placement error resulted in added displacement vectors of 5.12 nm in $x$ and 3.56 nm in $y$. Further work will be required to drive down image placement errors in order to meet the ITRS roadmap for imprint masks. Resolution after pattern transfer of 28 nm has been confirmed. The early results on both etch depth and CD uniformity are promising, but more extensive work is required to characterize the pattern transfer process.

The final subject to address is defectivity. Previous imprinting tests on wafer imprint tools indicates that particle adders of 0.1 per wafers pass can be obtained. A careful inspection of the replica blank in addition to low particle adders will be necessary to meet the aggressive defect targets necessary for replica mask fabrication.

### *Acknowledgments*

The authors would like to thank Masaaki Kurihara, Shiho Sasaki, Koji Ichimura, and Naoya Hayashi from Dai Nippon Printing for their excellent imprint mask fabrication work.

### *References*

1. M. Colburn, S. Johnson, M. Stewart, S. Damle, T. Bailey, B. Choi, M. Wedlake, T. Michaelson, S. V. Sreenivasan, J. Ekerdt, and C. G. Willson, *Emerging Lithographic Technologies III, Proc. SPIE* **379**, 379–389 (1999).
2. M. Colburn, T. Bailey, B. J. Choi, J. G. Ekerdt, and S. V. Sreenivasan, *Solid State Technol.* **44**(7), 67–76 (2001).
3. T. C. Bailey, D. J. Resnick, D. Mancini, K. J. Nordquist, W. J. Dauksher, E. Ainley, A. Talin, K. Gehoski, J. H. Baker, B. J. Choi, S. Johnson, M. Colburn, S. V. Sreenivasan, J. G. Ekerdt, and C. G. Willson, *Microelectron. Eng.* **61–62**, 461–467 (2002).
4. R. S. Sasaki, T. Hiraka, J. Mizuochi, A. Fujii, Y. Sakai, T. Sutou, S. Yusa, K. Kuriyama, M. Sakaki, Y. Morikawa, H. Mohri, and N. Hayashi, *Proc. SPIE.* **7122**, 71223P (2008).
5. S. V. Sreenivasan, P. Schumaker, B. Mokaberi-Nezhad, J. Choi, J. Perez, V. Truskett, F. Xu, and X, Lu, presented at the SPIE Advanced Lithography Symposium Conference, (2009).
6. K. Selenidis, J. Maltabes, I. McMackin, J. Perez, W. Martin, D. J. Resnick, and S. V. Sreenivasan, *Proc. SPIE* **6730**, 67300F (2007).
7. I. McMackin, J. Choi, P. Schumaker, V. Nguyen, F. Xu, E. Thompson, D. Babbs, S. V. Sreenivasan, M. Watts, and N. Schumaker, *Proc. SPIE* **5374**, 222–231 (2004).
8. L. Singh, K. Luo, Z. Ye, F. Xu, G. Haase, D. Curran, D. LaBrake, D. Resnick, and S. V. Sreenivasan, *Proc. SPIE* **7970**, 797007 (2011).
9. M. Melliar-Smith, S. V. Sreenivasan, and D. J. Resnick, "Jet and flash imprint lithography for high volume manufacturing," presented at the Sematech Litho Forum, May 10–12, 2010.
10. S. Sasaki, T. Hiraka, J. Mizuochi, Y. Sakai, S. Yusa, Y. Morikawa, H. Mohri, and N. Hayashi, *Proc. SPIE* **7470**, 74700J (2009).
11. T. Hiraka, J. Mizuochi, Y. Nakanishi, S. Yusa, S. Sasaki, Y. Morikawa, H. Mohri, and N. Hayashi, *Proc. SPIE* **7379**, 73792S (2009).
12. G. M. Schmid, C. Brooks, Z. Ye, S. Johnson, D. LaBrake, S. V. Sreenivasan, and D. J. Resnick, *Proc. SPIE* **7488**, 748820 (2009).
13. Z. Ye, R. Ramos, C. B. Brooks, P. Hellebrekers, S. Carden, and D. LaBrake, *Proc. SPIE* **7637**, 76371A (2010).
14. D. J. Resnick, G. Haase, L. Singh, D. Curran, G. M. Schmid, K. Luo, C. Brooks, K. Selinidis, J. Fretwell, and S. V. Sreenivasan, *Proc. SPIE* **7637**, 76370R (2010).
15. K. Selinidis, E. Thompson, S. V. Sreenivasan, D. J. Resnick, M. Pritschow, J. Butschke, M. Irmscher, H. Sailer, and H. Dobberstein, *Proc. SPIE* **7379**, 73790N (2009).
16. E. E. Moon, J. Lee, P. Everett, and H. I. Smith, "Application of interferometric broadband imaging alignment on an experimental x-ray stepper," *J. Vac. Sci. Technol. B* **16**(6), 3631–3636 (1998).
17. I. McMackin, P. Schumaker, D. Babbs, J. Choi, W. Collison, S. V. Sreenivasan, N. E. Schumaker, M. P. C. Watts, and R. D. Voisin, *Proc. SPIE* **5037**, 178–186 (2003).
18. M. Malloy and L. C. Litt, *Proc. SPIE* **7637**, 763706 (2010).
19. G. M. Schmid, N. Khusnatdinov, C. B. Brooks, D. LaBrake, E. Thompson, and D. J. Resnick, *Proc. SPIE* **7028**, 70280A (2008).
20. C. Brooks, K. Selinidis, G. Doyle, L. Brown, D. LaBrake, D. J. Resnick, and S. V. Sreenivasan, *Proc. SPIE* **7823**, 78230O (2010).

Biographies and photographs of the authors are not available.